Laser-driven hydrodynamic perturbation in an overdense Z-pinch plasma[a)]

John G. Ackenhusen[b)] and David R. Bach

Laser Plasma Interaction Laboratory, The University of Michigan, Ann Arbor, Michigan 48109
(Received 23 March 1978; accepted for publication 3 October 1978)

Holographic interferometry of the interaction of a radially incident intense CO_2 laser beam (10^{11} W/cm^2, 38-nsec FWHM pulse) with an overdense helium Z-pinch plasma ($n_e > 10^{19}$ e/cm^3, $T_e \sim 20$ eV, $L = 100$ μm) has indicated the presence of a laser-driven shock. The radial dimension of the shock was found to be similar to the electron thermal conduction length, several times larger than the focal-spot dimension. Density structure within the shock was inferred from holographic interferograms. Heuristic considerations of the shock density ratio, the front thickness, and the shock velocity allowed for an estimate of 50–80% energy absorption.

PACS numbers: 52.25.Ps, 52.50.Lp, 52.40.Db, 52.50.Jm

I. INTRODUCTION

An intense focused pulse of electromagnetic radiation may induce substantial hydrodynamic perturbation in a target placed at beam focus. For a solid target irradiated at sufficiently high intensity, the resulting energy deposition ionizes the focal region and forms a plasma that may blow off the solid surface and toward the laser, leaving a crater larger than the focal spot size. In current theoretical models,[1–3] the hydrodynamic behavior governing heating and motion of target material is determined by easily estimated characteristic scale lengths. The ratio of characteristic plasma length to energy absorption length, or the Bouguer number, is important in determining whether the resulting hydrodynamic motion is characterized by uniform flow from the region or instead by the formation of a laser-driven shock. Also important in this determination are the ratio of thermal conduction of energy flux from the region to laser energy flux into the region, and the diameter of the focal spot relative to the thermal conduction length.[2] These ratios determine regimes which are distinguished by differing theoretical scaling of final temperature, flow velocity, and perturbation size with incident intensity.

We report results of an interferometric investigation of a laser-matter interaction taken in the "thick deflagration" regime (i.e., short absorption length and high energy flux) in which a laser-driven shock and deflagration are observed. Other experiments in this regime have been performed on solid targets.[2,3] This experiment differs in that an independently created fully ionized plasma, produced by a Z-pinch discharge, comprises the target. As a result, the target plasma can be diagnosed in the absence of the laser to determine the initial conditions and to differentiate between discharge effects and laser effects. Additionally, because the target is fully ionized before laser incidence, ionization effects such as laser-supported detonation waves and material energy levels may be ignored.

II. EXPERIMENTAL ARRANGEMENT

The plasma was produced by a low-inductance coaxial Z-pinch discharge.[4] This provided a vertical plasma column that reached a peak density of 4×10^{19} e/cm^3 (four times the critical density for 10.6-μm radiation), and which had a critical scale length ($L = n_c/\nabla n_e$) as short as 70 μm. A separate paper[5] elaborates upon the density behavior of the plasma as

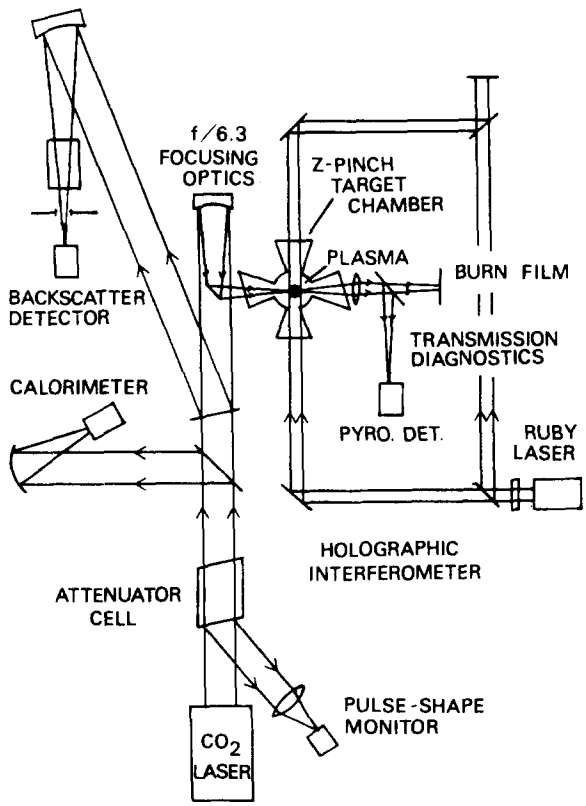

FIG. 1. Experimental arrangement. Holographic interferometer object beam and CO_2 laser beam are mutually perpendicular and impinge radially on the Z-pinch plasma column.

[a)]Supported in part by the National Science Foundation, the Air Force Office of Scientific Research, and The University of Michigan College of Engineering.
[b)]Permanent address: Bell Laboratories, Murray Hill, N.J. 07974.

 0021-8979/79/042623-07$01.10

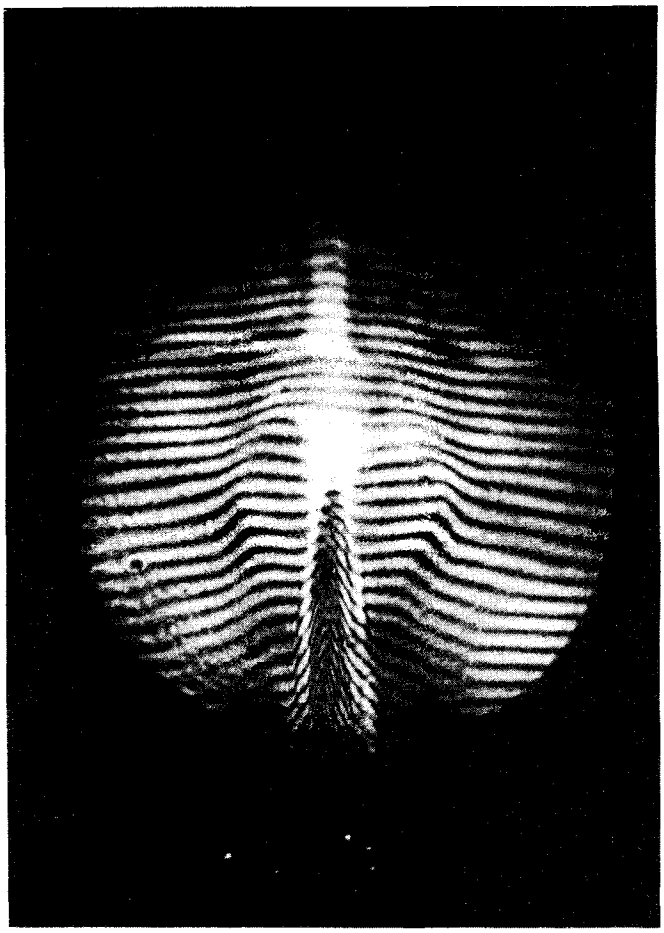

FIG. 2. Reconstructed holographic interferogram. CO_2 laser is incident on underdense plasma column. Laser beam enters from right of picture and has blown out the plasma column at axial position of incidence.

a function of time due to Z-pinch dynamics. A variety of diagnostics indicated an electron temperature of around 20 eV at the time of peak density. The plasma ion species was entirely He^{2+}.

The beam from a CO_2 TEA laser was focused to a diffraction-limited spot 125 μm in diameter and impinged radially upon the plasma column (Fig. 1). The laser pulse was 10.6 μm in wavelength, 38 nsec full width at half maximum (FWHM), and, for the shots discussed in this paper, was at a peak focused intensity of 10^{11} W/cm^2 $\pm$ 20%. Also shown in Fig. 1 are diagnostics to examine any transmitted 10.6-μm radiation, used in an investigation of nonlinear laser-plasma interactions.[6,7]

The object arm of a pulsed holographic interferometer[8] viewed the plasma column radially and at 90° to the axis of the CO_2 laser beam. The interferometer laser pulse, 16 nsec FWHM, was from a frequency-doubled ruby laser with a wavelength of 347.2 nm.

Abel inversion of the shift of moiré fringes placed on the double-exposure interferogram allowed the determination of electron density for the axisymmetric plasma. The spatial half-period of the moiré fringes was 160 μm, which assured that all laser-induced perturbations recorded interferometrically were macroscopic hydrodynamic effects, that is, larger than the focal-spot size of 125μm.

The time scale of the plasma-density evolution was sufficiently slow to allow a nearly stationary target profile during the time of the 38-nsec laser pulse.[5] However, the target-density profile was very dependent upon the time of laser incidence relative to time of plasma pinch. In addition, since the results of the laser-induced perturbation were recorded by the interferometer pulse, knowledge of timing between the two laser pulses was essential to follow the evolution of the perturbation. The time of peak plasma density was marked by a pulse of optical continuum radiation from the discharge. This was used to time the two laser pulses to a constant stage of discharge evolution on successive shots. Timing between the two laser pulses was determined by mixing the CO_2 detector signal and a passively delayed interferometer detector signal in a common information channel. Thus, the lasers were timed relative to pinch to within 10 nsec and relative to each other to within 4 nsec.

III. RESULTS

Before discussing the results of interactions in the deflagration regime, it is useful to examine an interferogram of the CO_2 laser incident on the plasma at an early stage of the

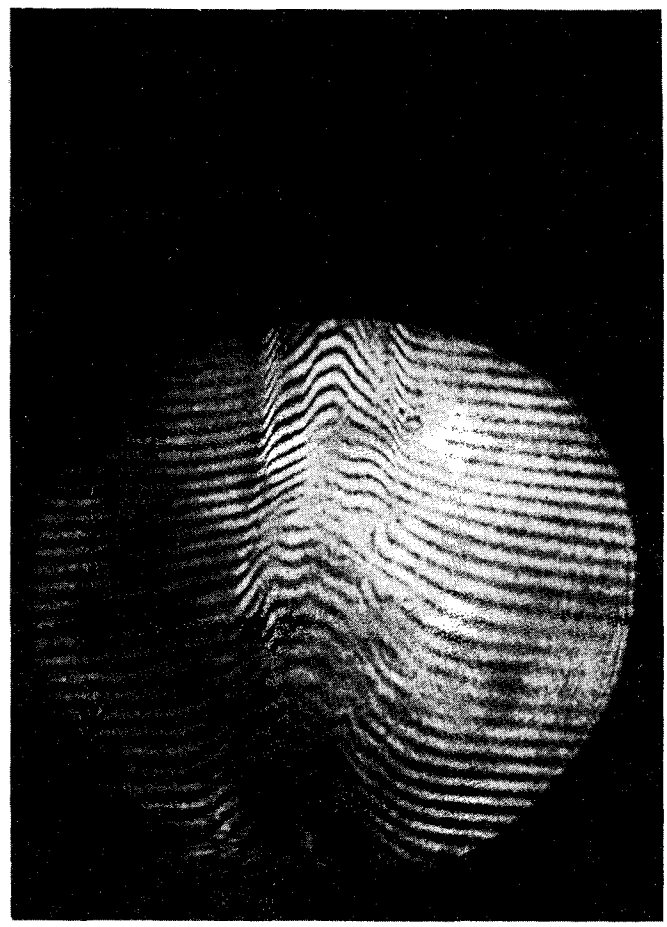

FIG. 3. Reconstructed holographic interferogram of plasma near pinch (overdense) and 10 nsec before peak of the 38-nsec FWHM CO_2 laser pulse. The fringe "twitch" at the right of column, one-third down, indicates the initiation of hydrodynamic perturbation.

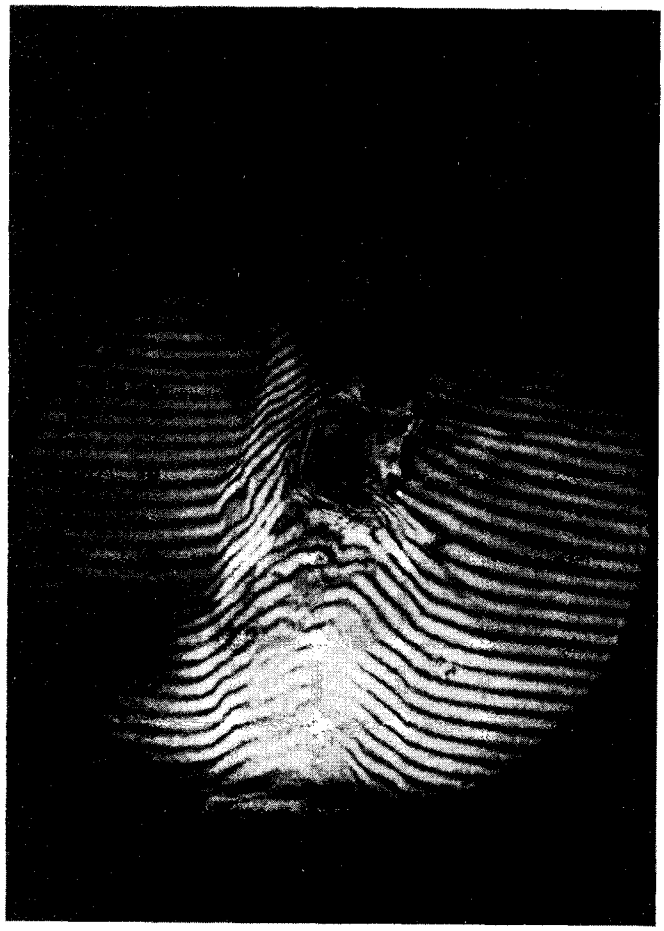

FIG. 4. Reconstructed holographic interferogram taken at peak of CO_2 laser pulse incident on overdense plasma. The laser-driven shock has propagated about halfway across the column.

Z-pinch evolution, before the critical density is reached. In this case, the radiation absorption length is comparable to the plasma dimension, resulting in a uniform plasma flow out of the irradiated region. Figure 2 displays an interferogram taken with the CO_2 laser incident on an underdense plasma column. The laser beam enters from the right at about one-third of the way down from the top of the column. The steeply rising moiré fringes at the bottom of the column indicate a peak centerline density of about 5×10^{18} e/cm^3 in contrast to that of the blown-out segment at less than 1×10^{18} e/cm^3. The region of blow-out is about 0.8 mm wide, much larger than the 0.125 mm focal-spot size.

A. Laser-driven shock

For an overdense target plasma, the presence of a critical layer results in a very short absorption length, placing the interaction in the deflagration regime previously discussed. A series of three interferograms presents the evolution of a laser-induced shock wave. Figure 3 displays the plasma column 6 nsec before peak compression. The position and direction of laser incidence is identical to that of Fig. 2. This interferogram was taken 10 nsec before the peak CO_2 laser intensity was reached and one may note the beginning of a laser-induced perturbation at the right of the column. The small area of fringe doubling indicates the beginning of plasma motion in the direction of the beam propagation, leading to a density shock front.

Figure 4 shows this shock wave 10 nsec later in an interferogram coincident with the peak of the CO_2 laser pulse. At the axial position of the interaction, three distinct regions are visible. Moving from right to left, the first region is a low-density region resulting from the driving of mass into the second region. This second region, forming a border of closely-space moiré fringes about the cavity like first region, is the high-density shock front. To the left of the front is the third region, containing an unperturbed fringe pattern, as yet undisturbed by the propagating shock. Figure 5 presents a sketch of the three regions and the density dependence within the regions.

An interferogram of the perturbation taken at the turn-off of the laser pulse, 38 nsec after Fig. 4, shows that the shock front has expanded axially (Fig. 6).

B. Extraction of densities from perturbation

To further study the properties of the laser-induced shock, it was necessary to obtain an estimate of the electron density in the perturbed region. The simple axial symmetry used in Abel inversion did not apply in the perturbed region, as the symmetry was destroyed by the radially incident one-sided perturbation. The perturbed region was asumed to be symmetric about the axis of the incident laser beam. As suggested by the rectangular shape of the cavity (deflagration region) and its border (shock front) in Fig. 4, the cavity and border were modeled as bounded by nested cylinders centered on the axis of laser incidence. Figure 7 shows the geometry associated with this analogy.

At the axial position of the centerline of the incident beam, the shock front was treated as a slab of length $2L$ imbedded in a vertical cylinder (the plasma column). The phase change of an object ray which passes through the high-density front (shaded portion of diagram) at this height was

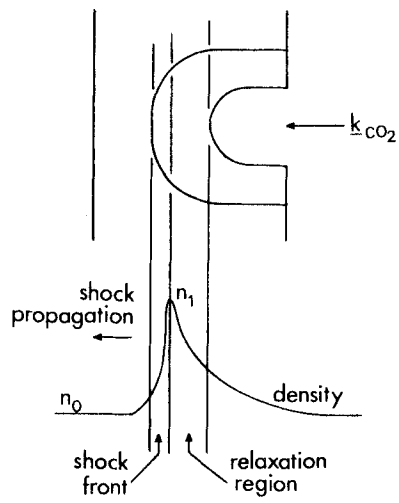

FIG. 5. Features of shock structure for interferogram of Fig. 4, relating shock regions to portions of perturbation in interferogram.

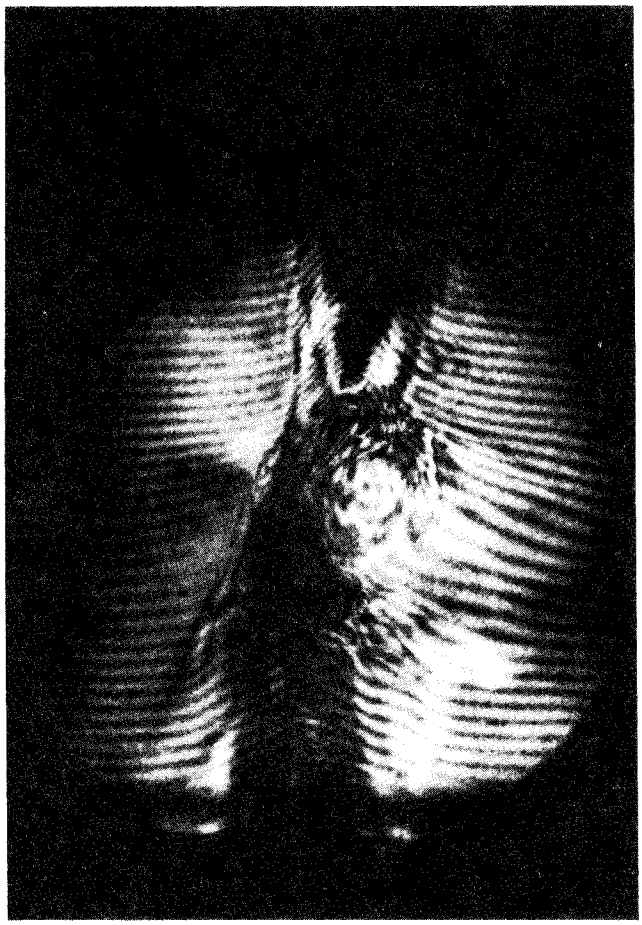

FIG. 6. Reconstructed holographic interferogram taken at end of CO_2 laser pulse, showing expanded shock front.

separated into a contribution from the unperturbed axisymmetric region and the slab like shock front perturbation of length $2L$. The optical path through the unperturbed portion was determined by a measurement at a radius z_0 in the unperturbed left region of the column, and then subtracted to determine the optical path, and thus the density, within the shock.

Figure 8 presents the electron density as a function of r taken at the axial position of the incident CO_2 laser beam (solid line). The density profile at the axial position just above the upper boundary of the perturbed region is also displayed (dotted line) to allow comparison of the perturbed and unperturbed density plots. The six data points to the immediate left of the vertical axis represent densities extracted by the combined slab and cylindrical geometries just described. The vertical dashed line is drawn at the leading edge of the shock front and defines the border between the perturbed and unperturbed regions. The remaining points were obtained by the more conventional Abel inversion of the axisymmetric unperturbed region.

Before further discussing the features of the shock wave, an attempt to verify the density step in the shock front by some simple comparisons is useful to check the technique. For a shock front of size and density profile as indicated in Fig. 8, the total number of particles within the front can be calculated. A particle conservation calculation indicates that the increase in the number of particles in the shock front over that in the unperturbed profile is within 10% of the decrease in particles in the deflagration region.

The right-hand side of the interferogram indicates a very small amount of mass blow-off toward the laser; a two-dimensional analytical calculation[9] of mass blow-off for a concentrated impact on a slab surface indicates less than 5% mass blow-off toward the laser.

C. Estimate of energy absorption

The portion of the plasma column that coincided with the beam path of the CO_2 laser was imaged on an aperture and then reimaged on a pindiode light detector. Thus, the detector viewed only the optical emission from the focal volume of the plasma. A comparison of the optical pulse shape from the plasma for a laser incident on an underdense plasma [Fig. 9(a)] to that for laser incident on an overdense plasma [Fig. 9(b)] indicated an enhancement in continuum emission for the illuminated overdense plasma. The 150-nsec FWHM pulse of the underdense target was identical in shape and intensity to the burst of optical radiation at time of peak compression in the absence of laser illumination, and, thus, was a feature of plasma dynamics rather than laser heating. The narrower more intense pulse for an overdense laser target evidently was composed of a sharp 40-nsec burst

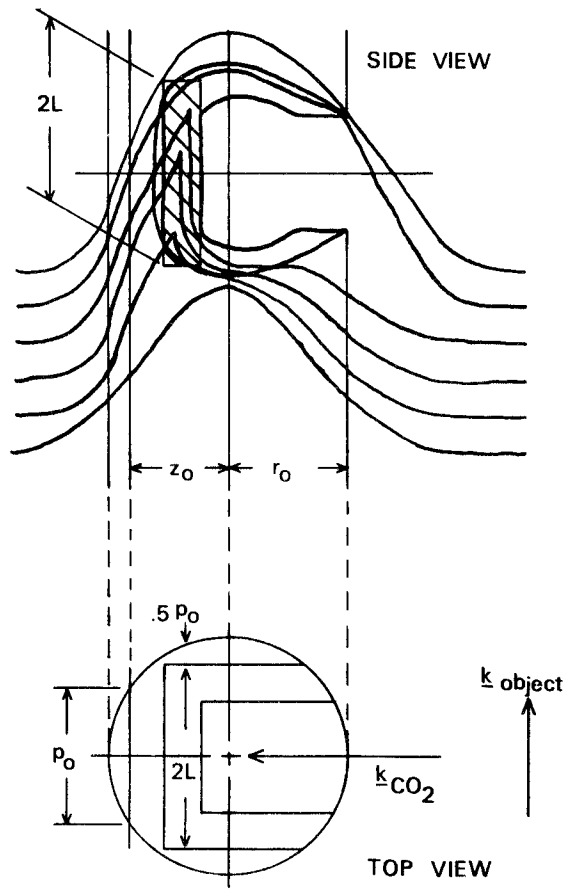

FIG. 7. Geometry of shock front used in extraction of densities along axial position of CO_2 laser beam.

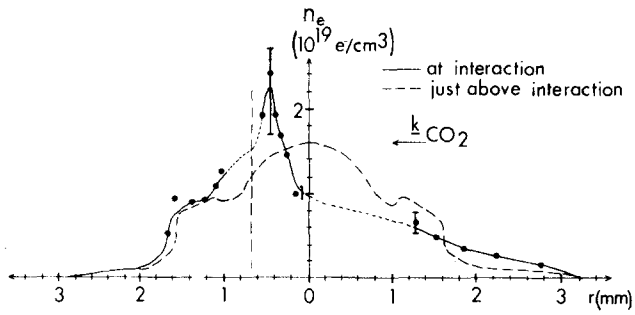

FIG. 8. Comparison of unperturbed density profile (dashed line), extracted just above perturbed region of Fig. 4, to laser-perturbed density profile, extracted along line at height of centerline of perturbation (position of laser beam center).

associated with laser heating superposed on the wide optical pulse associated with plasma dynamics.

To quantify the energy transfer from the beam to the plasma proved quite difficult. An initial attempt to diagnose x-ray continuum emission due to plasma heating proved fruitless—a calculation indicated that the small interaction volume would require heating to 200 eV before emitting detectable x-ray energy.

Several estimates of energy deposition were performed utilizing density structure and velocity of the laser-driven shock. One such estimate used the Taylor-Sedov expression for the time dependence of the radius of a spherically expanding shock, $R(t)$. The radius of the shock is expressed as a function of time t, initial average mass density ρ_0, and deposited energy Q by the expression

$$R(t) = \xi_0 (Q/\rho_0)^{1/5} t^{2/5}, \tag{1}$$

where $\xi_0(\gamma) = 1.12$ for a specific-heat ratio γ equal to 5/3. For the shot of Fig. 4, taken coincident with the peak of the laser pulse, the shock had penetrated 1.5 mm into the column and had reached that stage 19 nsec into the 38-nsec FWHM laser pulse, implying an average front velocity of 8×10^6 cm/sec. Although this scheme of estimating energy absorption has worked well in spherical geometries,[10] it is questionable in this geometry. Additionally, the self-similar analysis used is within the strong-shock limit (density ratio of 4 for $\gamma = 5/3$) and for an explosive energy deposition. Therefore, an attempt at an independent verification was made.

The Hugoniot relation for a planar shock with an external energy source expresses the pressure ratio across a shock, p_1/p_0, in terms of the deposited energy Q and the specific volumes V_1 and V_0 (subscript 0 refers to region ahead of shock; 1 refers to shock front).[11] This relation, when combined with the ideal gas law, expresses the deposited energy in terms of the measured quantities V_0, V_1, and initial temperature θ_0:

$$Q = (\theta_0/2V_0)\{V_0/V_1[(\gamma+1)V_1 - (\gamma-1)V_0] - (\gamma+1)V_0 + (\gamma-1)V_1\}. \tag{2}$$

A third argument may be made utilizing the theory of weak shocks to equate the measured shock-front thickness to the thermal mean free path, in turn a function of temperature.[12] The thermal-energy increase in the front region is then summed with the kinetic energy associated with driving particles from the cavity region to the shock front during the laser pulse.

These three heuristic arguments provided similar estimates of the energy-absorption fraction. It was concluded that energy absorption ranged between 50 and 80% of the incident beam energy, with the wide range due to the uncertainty inherent in the shock density determination and the severe simplification of the experimental situation to fit these arguments. However, a more refined and direct measurement of energy absorption is required, and future efforts with light-scattering diagnostics are expected to prove more accurate.

IV. DISCUSSION

A comparison of the interferogram of Fig. 2, in which the peak plasma density is well below the critical density at the time of laser irradiance, with the interferograms of Figs. 3, 4, and 6, in which the target plasma was overdense at the time of laser irradiation, indicates the effect of the radiation absorption length upon the resultant plasma motion. For the shot of Fig. 2, the peak plasma density was 5×10^{18} cm^3. In this situation, the dominant means for energy transfer from the laser beam to the plasma is inverse bremsstrahlung. The radiation absorption length $1/K^{IB}$, where K^{IB} is the absorption coefficient for inverse bremsstrahlung, is about 0.5 mm,

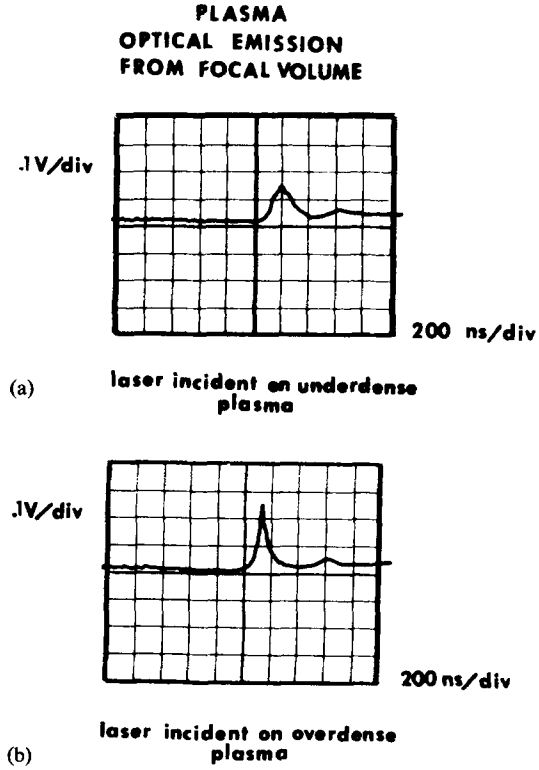

FIG. 9. Oscilloscope traces showing enhanced optical continuum emission for (b) laser incidence on an overdense target plasma over (a) that associated with discharge dynamics.

comparable to the plasma radius. In this regime, laser radiation is absorbed fairly uniformly across the plasma column resulting in uniform expansion and the flow of plasma from the heated region as shown in the interrupted column structure of Fig. 2.

In the other three interferograms, the peak electron density is several times the critical density for the 10.6-μm laser radiation, and as a result, a critical layer and a short critical-density scale length ($L = 100\,\mu$m) are presented to the beam. The laser energy is deposited in a very thin lamina compared to the plasma column dimension. This results in the shock-deflagration structure seen in the interaction region. The structure and size of the perturbation is dependent upon the portion of the laser energy removed from the focal-spot region by thermal conduction or convective motion.

To determine the magnitude of the convective and conductive energy flux from the region of irradiation relative to the incident laser flux into the region, some simple scaling arguments are presented.

Energy from the laser is deposited by a combination of inverse bremsstrahlung and non classical absorption in a thin region near the critical layer. Energy is removed from the interaction region by convective motion and thermal conduction.[2,3] Energy flux out of the region Φ_{out} may thus be represented as

$$\Phi_{\text{out}} = c_0(E_{\text{thermal}} + E_{\text{kinetic}}) - K\nabla\theta_e, \tag{3}$$

where c_0 is the flow velocity, E_{thermal} is the plasma thermal energy in the heated region given by

$$E_{\text{thermal}} = \frac{5}{2}(n_e\theta_e + n_i\theta_i), \tag{4}$$

E_{kinetic} is the plasma kinetic energy due to directed motion

$$E_{\text{kinetic}} = \frac{1}{2}(m_i n_i + m_e n_e)c_0^2, \tag{5}$$

and K is the electron thermal conductivity. The electron (ion) density is n_e (n_i), the electron (ion) mass is m_e (m_i), and the electron and ion temperatures in energy units are θ_e and θ_i. The electron-ion equilibration time is 1–2 nsec; therefore, the electron and ion temperatures may be treated as equal on the longer time scale of the laser pulse. Energy flux into the region is given by the laser intensity, $\Phi_{\text{in}} = 10^{11}$ W/cm^2. The ratio of the convective flux out of the region to the laser energy flux into the region may now be calculated to be less than 10^{-5}. Thus, energy is absorbed from the laser beam much more rapidly than it can be convected away by plasma motion, and the convective flux may be ignored when compared to the radiative flux.

Turning now to the energy flux removed from the interaction region by thermal conduction, a thermal conduction length, l, may be defined as that length over which the thermal conductive flux is comparable to the convective flux. This length may be calculated by equating the conductive and convective terms in the expression for Φ_{out}, the total flux removed from the region.[2] Thus,

$$K\theta_e/l \approx c_0(E_{\text{thermal}} + E_{\text{kinetic}}). \tag{6}$$

Using the thermal conductivity expression of Spitzer,[13] a value for l is found to be $l \approx 0.6$ mm.

The thermal conduction length l is large compared to the focal-spot radius of $\approx 60\,\mu$m. In this regime, known as the thick deflagration,[2] a shock is predicted to exhibit a radial dimension approximating l. The radius of the perturbation is measured from the interferograms to be approximately 0.7 mm, indeed similar to l. It should be stressed that l is a dimension of macroscopic hydrodynamic motion; diagnostics of transmitted laser radiation have suggested an additional density depression in the form of a hard aperture of dimension comparable to that of the focal spot, burned through the critical layer.[6,7]

As indicated by the interferogram taken at the end of the laser pulse (Fig. 6), expansion and flow from the interaction region occur primarily in the axial direction, perpendicular to the direction of the beam propagation. This asymmetry has been theoretically predicted in the thick-deflagration regime.[2] Additional asymmetry may occur as a result of the circumferentially directed magnetic field associated with the current through the discharge plasma. In the analysis, no account was taken of the effect of this field upon transport coefficients. An inhibition of transport across the magnetic field lines would be expected to result in differing expansion velocities in the axial and radial directions, and a constriction of the current-carrying plasma column due to the shock structure would serve to increase the discharge magnetic field in the interaction region. However, the time scale for plasma-column disassembly due to an $m = 0$ or $m = 1$ instability is over a factor of 10 larger than the laser-pulse length.

V. SUMMARY

The interaction of an intense beam of 10.6-μm electromagnetic radiation with an overdense plasma has been observed to result in a macroscopic hydrodynamic perturbation. The perturbation exhibits the structure of a laser-driven shock, and exhibits a characteristic dimension similar to the electron thermal conduction length in the region. Density information within the shock structure has been extracted by holographic interferometry and used to relate the density ratio across the shock, its front, its thickness, and its velocity to an estimate of energy absorbed from the laser. The formation of the shock has been shown to depend upon the condition of a radiation absorption length much shorter than the plasma dimension.

ACKNOWLEDGMENTS

We are grateful for useful theoretical discussion with Dr. J. Duderstadt, Dr. R. Ong, and Dr. R. Osborn, and thank Dr. P. Rockett, Dr. D. Steel, D. Brower, D. Kania, and D. Voss for essential experimental advice and assistance.

[1] R.G. Rehm, Phys. Fluids **13**, 921 (1970).
[2] P.E. Dyer, D.J. James, G.J. Pert, S.A. Ramsden, and M.A. Skipper, in *Laser Interaction and Related Plasma Phenomena*, Vol. 3A, edited by H.J.

Schwartz and H. Hora (Plenum, New York, 1974) p. 191.
[3]C. Fauquignon and F. Floux, Phys. Fluids **13**, 386 (1970).
[4]D.G. Steel, P.D. Rockett, D.R. Bach, and P.L. Colestock, Rev. Sci. Instrum. **49**, 456 (1978).
[5]John G. Ackenhusen and David R. Bach, J. Appl. Phys. **50**, 2956 (1979).
[6]P.D. Rockett, D.G. Steel, J.G. Ackenhusen, and D.R. Bach, Phys. Rev. Lett. **40**, 649 (1978).
[7]John G. Ackenhusen and David R. Bach, Appl. Phys. Lett. (to be published).
[8]P.D. Rockett, Ph.D. dissertation (University of Michigan, 1977) (unpublished).
[9]Y.B. Zel'dovich and Y.P. Raizer, *Physics of Shock Waves and High-Temperature Hydrodynamic Phenomena* (Academic, New York, 1966), p. 834.
[10]T.A. Leonard and F.J. Mayer, J. Appl. Phys. **46**, 3562 (1975).
[11]Y.B. Zel'dovich and Y.P. Raizer, Ref. 9, p. 50; Derivation also discussed, but final result incorrect, in T.P. Hughes, *Plasmas and Laser Light* (Wiley, New York, 1975).
[12]Y.B. Zel'dovich and Y.P. Raizer, Ref. 9, p. 75 and 515.
[13]L. Spitzer, *Physics of Fully Ionized Gases* (Wiley, New York, 1962), p. 144.